Elastic AWI and RWI in the Santos basin

Tenice Nangoo, Nikhil Shah, Adrian Umpleby, John Armitage, Mike Warner: S-Cube, London.*
Gustavo Catao Alves, Andre Bulcao, Analena Mileo Camara de Oliveira: Petrobras.

Summary

Acoustic full-waveform inversion is often able to build high-quality velocity models for sub-salt imaging using only acoustic wave propagation. This is achieved by adaptively matching acoustic data to the real-world elastic field data. Here we show both acoustic and elastic adaptive waveform inversion and reflection waveform inversion applied to salt-affected ocean-bottom node data from the Santos Basin, offshore Brazil. In this basin, the existence of high-velocity layered anhydrites within the salt generates elastic effects that appear sufficiently severe that full-elastic inversion is necessary in order to recover an adequate model. Combined RWI and elastic AWI are then able to generate a high-quality velocity model from raw hydrophone data that is sufficient for subsequent imaging using simple acoustic RTM.

Introduction

Full-waveform inversion now forms a near-essential part of velocity-model building for sub-salt imaging. Here, the role of FWI has evolved from its earliest use as an adjunct to conventional model building designed merely to sharpen an existing model, through several stages to become a complete technology able to build a full final velocity model without recourse to other technologies or human interpretation (Warner et al., 2023). Salt models invariably contain strong and rapid impedance contrasts, and these typically produce significant elastic effects in marine seismic data. Robust adaptive waveform inversion (AWI) (Guasch et al., 2019), kinematic reflection waveform inversion (RWI) (Warner et al., 2021), and related techniques, are nonetheless often able to generate high-accuracy high-resolution velocity models, cost-effectively, using only acoustic wave propagation.

Salt bodies in the Santos basin often contain anhydrite, or other high-impedance layers, at or close to their upper surfaces (Jouno et al., 2019). These fast layers can produce strong elastic effects in marine seismic data that even advanced schemes for matching acoustic and elastic data are unable to deal with completely. In such regions of the basin, full-elastic inversion appears to be necessary in order to generate an accurate velocity model even when hydrophone-only data are inverted and when no strong double-converted shear arrivals are apparent in the field data.

Elastic inversion can be much more expensive than acoustic inversion, partly because the associated vector wave equation involves more variables, partly because multi-parameter inversion typically requires an increased number of iterations and a more-expensive step-length calculation, but especially because a finer mesh size and shorter time step are required to model the slowest shear-waves accurately. Here we overcome these limitations during elastic FWI so that elastic inversion involves only two to three times the true computational cost of acoustic FWI.

The problem

Figure 1 shows hydrophone data from part of a single shot line through an ocean-bottom node lying above a large tabular stratified evaporite in the Santos basin. The maximum horizontal source-receiver offset in the figure is only 4800 m. The raw field data have been band-pass filtered between 2 and 22 Hz, and are displayed with trace normalization. No other processing has been applied.

The data show three principal labelled arrivals: (1) The earliest is the direct arrival, including its short-period surface ghost. The low-frequency bubble is apparent for several cycles behind the earliest arrival. The direct arrival is underlain by weak shallow reflections from the post-salt sedimentary section. (2) A p-wave reflection from the top of the evaporite sequence. This reflection is higher frequency than the direct arrival, and does not show a strong bubble signature at the shortest offsets, suggesting thin layering at or near the top of the salt section. Moving only a small distance away from zero offset, a significant phase rotation is apparent; the phase of the reflection rotates by almost 180° over a short distance. This rotation is apparent on data from many nodes, and is suggestive of strong elastic effects at top salt. (3) A fast, weak, low-frequency reflection from the base of the salt section is visible. This does show the low-frequency bubble pulse. This reflection is probably underlain by weak, slower, peg-leg-multiple reflections that occur between the top salt and the underside of the seabed.

Figure 2 shows simple one-dimensional modelling that reproduces some of these key features. The two synthetic records show acoustic simulations on the left, and elastic simulations on the right. The halite-only p-wave model contains water, above soft sediment, above a homogeneous halite layer. The “anhydrite above halite” model contains a thin fast anhydrite layer above the halite. The ratio of value of Vp to Vs ramps rapidly from about 4.5 at the seabed to 2.0 above the salt, and is 1.8 within the evaporites. The lowest value of Vs in the model is about 400 m/s; a similarly low value was used during elastic FWI. The lower portion of Figure 2 shows Zoeppritz absolute amplitude and unwrapped phase for p-p reflections from the top of the evaporites for these models.

Figures 2a and 2b show that, while there are important differences between the halite-only acoustic and elastic data, these involve principally only amplitude differences and reasonably benign phase rotations that are both amenable to adaptive matching during acoustic FWI. Consequently pure-acoustic AWI and RWI are capable of generating high-resolution high-accuracy kinematic models from most halite-dominated datasets. In contrast, Figures 2c and 2d, which best match the characteristics of the field data in Figure 1, show strong elastic effects at short offsets, with complex phase-behavior and phase reversals. These effects are normally beyond the capabilities of a generic adaptive acoustic inversion scheme without data-specific customization. Consequently, in order to invert such datasets successfully, fully elastic FWI is likely to be required.

The solution

By far the greatest increased cost of elastic FWI arises because of the short shear wavelength close to the seabed. Here, we are inverting only hydrophone data; these show no evidence for contamination by double-mode conversions. Using a suitably stable elastic propagator, we can then fully and correctly generate the observed pressure wavefield using a coarse mesh for which near-seabed shear-wave propagation is hopelessly compromised. Consequently, elastic FWI becomes affordable.

The second-greatest increase in cost often arises through the additional iterations and complications associated with elastic multi-parameter inversion. Here, we are not seeking to learn about the shear properties of evaporites or their overlying sedimentary cover. Consequently, all we require of the shear-model is that it correctly simulates the elastic portion of the p-wave amplitudes; the shear-model need not be highly accurate or spatially well-resolved to achieve this. Consequently, we do not invert for Vs; rather we maintain a fixed, smooth, relationship between Vp and Vs (and density) as elastic FWI proceeds, removing the need for, and cost of, multi-parameter inversion

We have further cost savings because the higher accuracy of elastic prediction means that we require fewer iterations to converge, especially in the presence of strongly elastic salt-related long-period multiples. And we are able to minimize the additional memory requirements of elastic FWI by aggressively compressing the stored forward wavefield. Consequently, the cost of elastic FWI is here less than three times the true cost of equivalent acoustic FWI.

Using this elastic scheme, we inverted hydrophone data from an array of around 1000 nodes, deployed in about 2.2 km of water, with a node spacing of about 350 m, and in-line and cross-line shot spacings of 50 m. The lowest usable frequency for FWI in these data was 2 Hz.

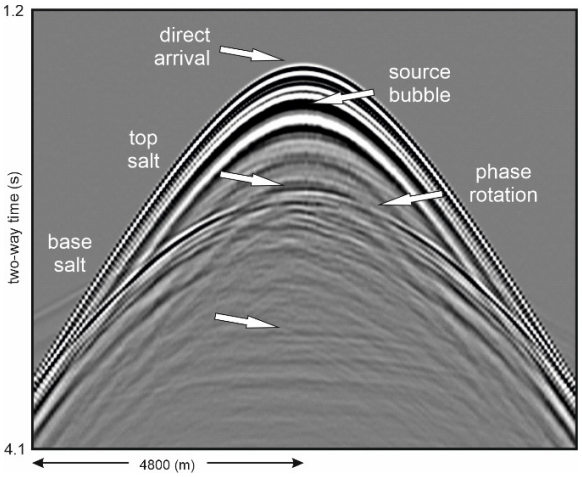

Figure 1: Short-offset portion of hydrophone data from a single shot line through an ocean-bottom node. The data are trace normalized, and band-pass filtered at 2-22 Hz.

The results

Figure 3 shows FWI p-wave velocity models and related reflectivity images from this dataset. The model is shown from 2 to 7 km depth; the color scale does not fully capture the detailed velocity structure recovered by FWI in the post-salt sequence. The base of salt is rather horizontal at about 5-km depth; predominantly carbonate velocities below the salt are high, and hydrocarbon reserves are contained in lower-velocity dipping sequences underlying the salt within the carbonates. The salt geometry is reasonably benign, but it is internally layered with strong velocity contrasts.

Figure 3a shows the start model for FWI; it is smooth and only includes an approximate location for top salt. A maximum offset of 16 km for the node data, combined with the high-velocity shallow evaporites, means that both refracted and reflected data are required by FWI to build velocity to 7-km depth. We began inversion at 2 Hz, applying acoustic AWI in the shallow section, and combined AWI and RWI in the deeper model. Figure 3b shows the results to 5.5 Hz. Despite the elastic features of the data, acoustic inversion has made useful progress, but the data fit is poor. Consequently, we reinitiated elastic FWI, without significant adaptive matching, beginning from the earlier 5-Hz acoustic model.

Figure 3c shows the result of elastic inversion run to 20 Hz. Spurious structure in the acoustic model now seems to have disappeared, and the low velocities associated with the hydrocarbon-bearing sediments are now captured with more accuracy. Base salt is clear, as are high-velocity presumed-anhydrite and similar layers within the salt. This model should now be sufficient for conventional RTM.

Figure 3d shows the FWI-derived normal-incidence p-wave primary reflectivity generated by differentiating the acoustic impedance obtained from the elastic FWI model. This provides directly an 20-Hz FWI-based non-linear least-squares elastic RTM image. Figure 3e shows the corresponding conventionally generated acoustic non-iterative RTM image at 45 Hz. The former image is recovered directly from raw unprocessed hydrophone-only data, whereas the latter image is generated using fully processed, PZ-summed, primary-only data. Apart from their obvious differences in bandwidth, the two images are similar. The FWI image is true amplitude.

Conclusions

While adaptive acoustic FWI can recover accurate high-resolution velocity models for many salt-affected data sets, under appropriate circumstances full-elastic FWI can prove to be both necessary and affordable. Accurate elastic p-wave amplitudes do not however require accurate propagation of s-waves on a fine mesh, so that elastic FWI is not then unduly expensive. In the Santos Basin, although the salt is structurally simple, fast layers within the salt do appear to require elastic FWI in order to recover an accurate velocity model; this approach appears to have worked well here.

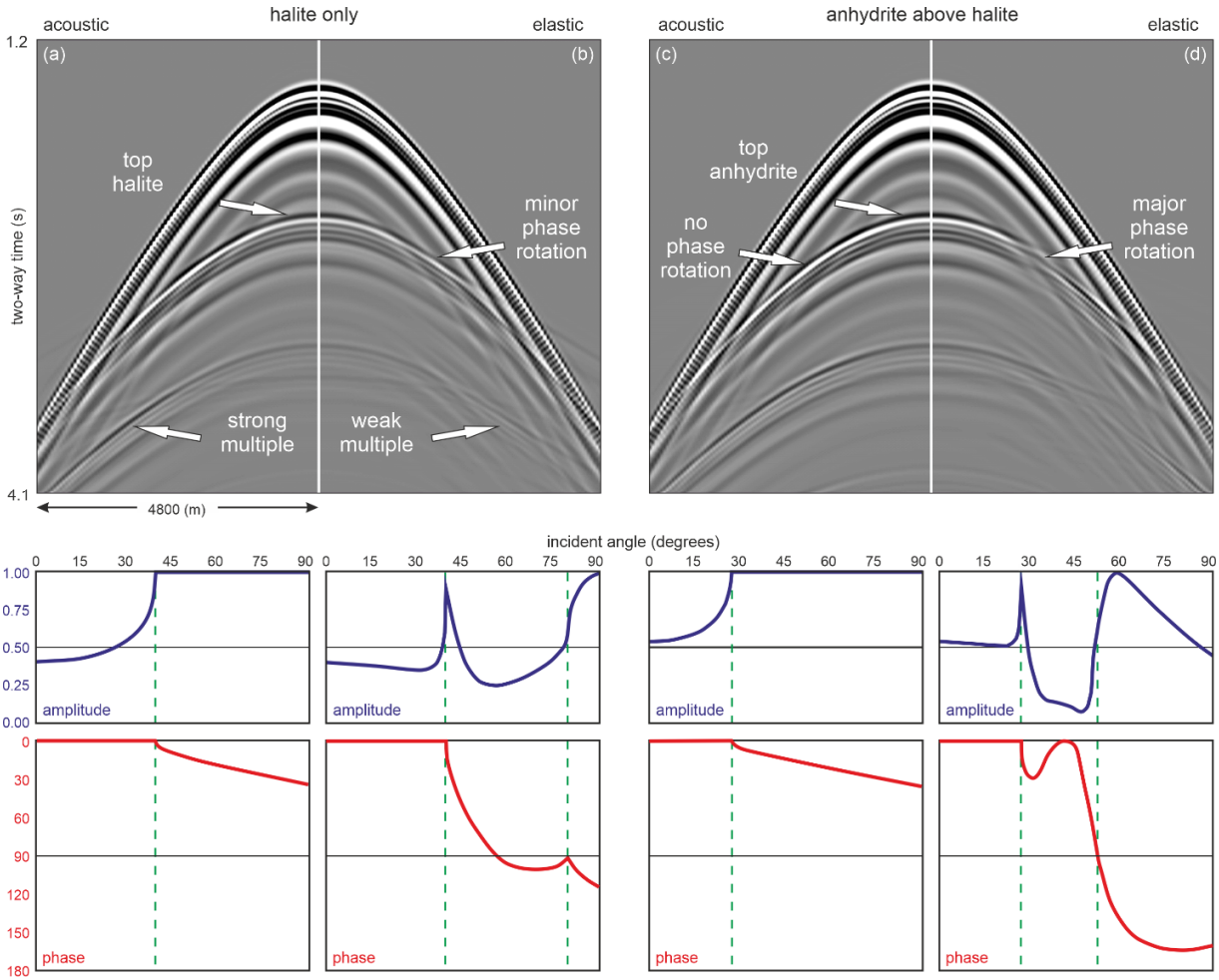

Figure 2: Synthetic data from four, simple, one-dimensional models (above), and corresponding pp-reflection amplitude and phase calculated using the isotropic Zoeppritz plane-wave equations (below). (a) Acoustic synthetics containing water, post-salt sediment, and pure halite. (b) The equivalent elastic synthetics. (c) Acoustic synthetics that includes a thin, fast, anhydrite layer at top salt. (d) The equivalent elastic synthetics.

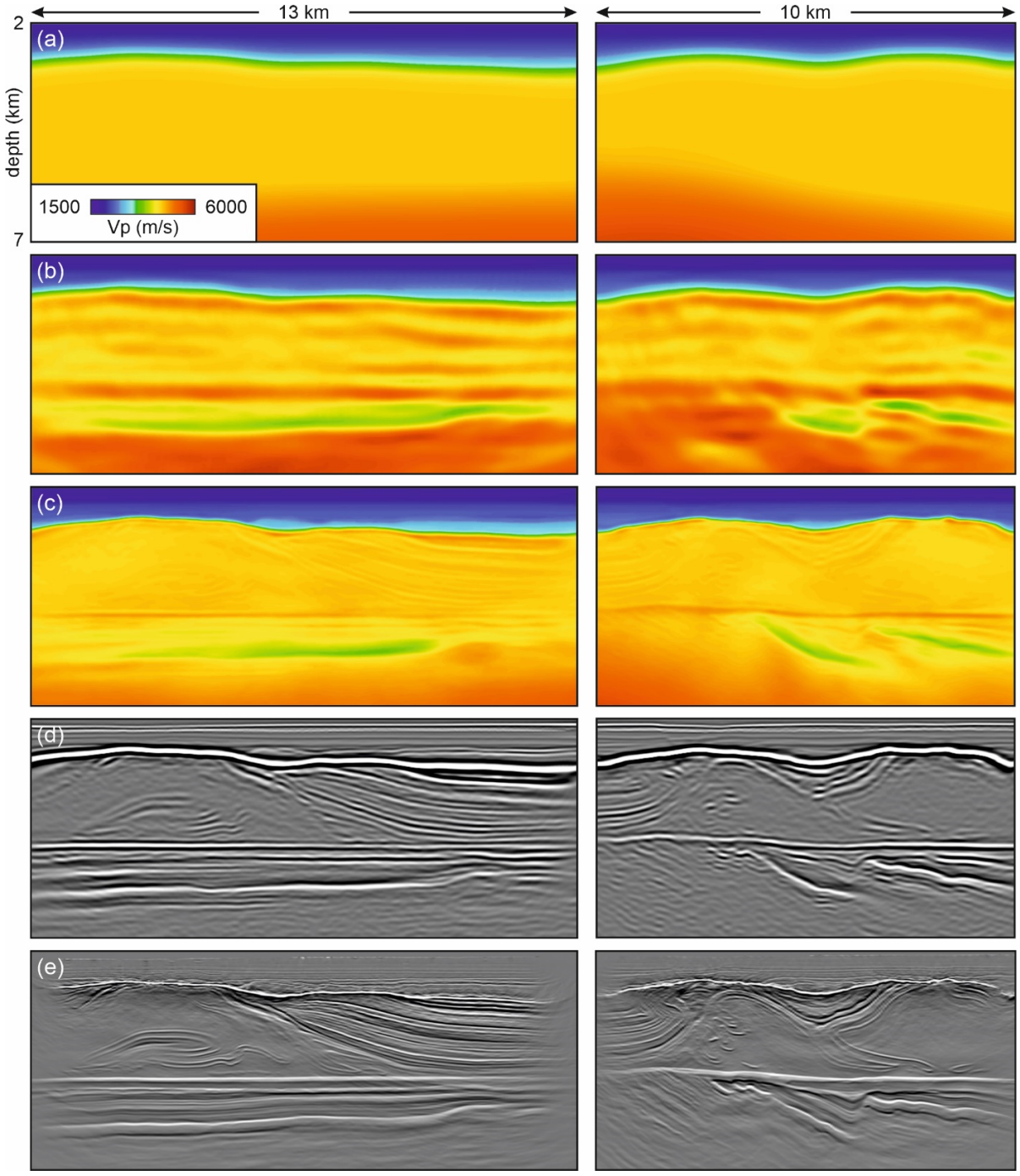

Figure 3: P-wave velocity models and reflectivity images. Left: in-lines in the sub-salt strike direction. Right: cross-lines in the sub-salt dip direction. (a) Starting model for FWI. (b) Acoustic inversion run to 5.5 Hz. The model is already failing. (c) Elastic inversion run to 20 Hz. High-velocity anhydrites appear as thin red lines. The base of the evaporite section is flat. (d) P-wave reflectivity image obtained by spatial differentiation of the elastic FWI acoustic-impedance model at 20 Hz. (e) Corresponding conventional acoustic RTM run to 45 Hz.